Research Article

Angewandte Chemie International Edition
www.angewandte.org

How to cite: *Angew. Chem. Int. Ed.* **2024**, *63*, e202408429
doi.org/10.1002/anie.202408429

Crystallization | Hot Paper

From Ions to Crystals: A Comprehensive View of the Non-Classical Nucleation of Calcium Sulfate

Matthias Kellermeier, Johanna Scheck, Markus Drechsler, Rose Rosenberg, Tomasz M. Stawski, Alejandro Fernandez-Martinez, Denis Gebauer,* and Alexander E. S. Van Driessche**

In memory of Helmut Cölfen

Abstract: The early stages of mineralization continue to be in the focus of intensive research due to their inherent importance for natural and engineered environments. While numerous observations have been reported for single steps in the pathways of various crystallizing phases in previous studies, the complexity of the underlying processes and their elusive character have left central questions unanswered in most cases. In the present work, we provide a detailed view on the nucleation of calcium sulfate mineralization—an abundant mineral with broad use in construction industry—in aqueous systems at ambient conditions. As experimental basis, a co-titration procedure with potentiometric, turbidimetric and conductometric detection was developed, allowing solution speciation and the formation of crystallization precursors to be monitored quantitatively as the level of nominal (super)saturation gradually increases. The nature and spatiotemporal evolution of these precursors was further elucidated by time-resolved small-angle X-ray scattering (SAXS) and analytical ultracentrifugation (AUC) experiments, complemented by cryogenic transmission electron microscopy (cryo-TEM) as a direct imaging technique. The results reveal how ions associate into nanometric primary species, which subsequently aggregate and develop anisotropic order by intrinsic structural reorganization. Our observations challenge the common understanding of fundamental notions such as the nucleation barrier or the meaning of supersaturation, with broad implications for mineralization phenomena in general and the formation of calcium sulfate in geochemical settings and industrial applications in particular.

Introduction

During the last decade, our understanding of crystallization processes has evolved substantially and the classical picture drawn by textbooks now appears to be more challenged than ever before.[1] Numerous studies on the formation of colloidal,[2,3] organic[4–6] and inorganic[7–15] crystals from solution have revealed that the mechanisms underlying nucleation and growth phenomena can be far more complex than traditionally believed, and may involve various pre-

[*] Dr. M. Kellermeier
Material Science
BASF SE
Carl-Bosch-Straße 38, D-67056 Ludwigshafen, Germany
E-mail: matthias.kellermeier@basf.com

Dr. J. Scheck, R. Rosenberg
Physical Chemistry
University of Konstanz
Universitätsstraße 10, D-78464 Konstanz, Germany

Dr. M. Drechsler
Bavarian Polymer Institute (BPI), Keylab "Electron and Optical Microscopy"
University of Bayreuth
Universitätsstraße 30, D-95440 Bayreuth, Germany

Dr. T. M. Stawski
Materials Chemistry
Federal Institute for Materials and Testing (BAM)
Richard-Willstätter-Straße 11, D-12489 Berlin, Germany

Dr. A. Fernandez-Martinez
ISTerre
Université Grenoble Alpes, Université Savoie Mont Blanc, CNRS, IRD, IFSTTAR
1381 Rue de la Piscine, F-38000 Grenoble, France

Prof. Dr. D. Gebauer
Institute of Inorganic Chemistry
Leibniz University Hannover
Callinstraße 9, D-30167 Hannover, Deutschland
E-mail: gebauer@acc.uni-hannover.de

Dr. A. E. S. Van Driessche
Instituto Andaluz de Ciencias de la Tierra (IACT)
CSIC-University of Granada
E-18100 Armilla, Granada, Spain
E-mail: alexander.vd@csic.es

cursors, either stable or metastable, which precede the final crystalline state and transform into one another at rates that intimately depend on the specific solution conditions. For an intensively investigated mineral system like calcium carbonate, species detected experimentally and/or predicted theoretically range from solute clusters in the initial one-phase system,[8,16–18] through heavily hydrated liquid-like droplets and pseudo-phases,[19–21] to amorphous and/or poorly crystalline nanoparticles with different possible structures,[13,22–25] all of which display dynamic (meta-)stabilities that change over time and as their size gradually increases.[26] Based on these observations, different crystallization pathways have been proposed; many current models assume that nucleation, growth and phase transformation proceed through progressive aggregation and coalescence of pre-formed units rather than continuous monomer addition,[27] likely due to kinetic reasons and driven by the reduction of interfacial free energies. However, for most systems investigated so far, only single snapshots of the overall pathway have been captured experimentally, owing to the stochastic nature of the process and the associated technical limitations in terms of spatial and temporal resolution. Thus, the thorough characterization of the complex sequence of steps leading from dissolved ions (or molecules) to mature crystals often poses a considerable experimental challenge, which has generated debates regarding the existence, nature and role of the primary species during the early stages of crystallization.[10,17,18,20,26,28] Similarly, the particular mechanisms underlying the transformation of a (less stable) disordered precursor to a (more stable) crystalline phase are still under discussion for different organic and inorganic materials.[29–31]

In the present work, we have studied the solution-mediated crystallization of calcium sulfate, a mineral system that has received much less attention in the recent literature[32,33] than for example calcium carbonates or phosphates, despite its inherent relevance for both industrial applications (e.g., as construction material[34] or undesired scale-forming compound[35]) and geochemical settings (e.g., as abundant deposits in evaporitic environments[36] or cloud condensation nuclei[37]). From a fundamental point of view, the $CaSO_4$ system bears the advantage of being considerably more soluble than the above-mentioned minerals, which leads to higher volume fractions of the species involved in nucleation that thus become more readily "observable".[38,39] Here we utilize this inherent benefit and combine a variety of advanced techniques for in situ experimental characterization, leveraging the advantages of real-time observation to capture transient intermediates and correlate structural changes with the physicochemical properties of the system. Our results show that the nucleation of gypsum ($CaSO_4 \cdot 2H_2O$, the stable phase at ambient conditions) starts with two populations of pre-associated nanoscopic species, which exist already in undersaturated solutions and assemble into larger disordered entities once a supersaturated state is reached. With time, order emerges in these undefined and highly transient domains, as individual building units align into one-dimensional chain-like structures. Progressively, these chains pack to build a proto-lattice, which upon densification ultimately becomes able to grow into relatively well-developed microscopic gypsum crystals. All these intriguing stages were directly visualized by means of cryo-transmission electron microscopy (cryo-TEM), while analytical ultracentrifugation (AUC) and small-angle X-ray scattering (SAXS) confirm the locally captured snapshots from an ensemble statistics point of view. Our results thus provide unprecedented insight into the full complexity of a "non-classical" multi-stage nucleation process and highlight how the emergence of anisotropy can pose additional intrinsic barriers to mineral formation from an isotropic intermediate phase.

Results and Discussion

In order to monitor calcium sulfate nucleation under controlled conditions and at a suitable time resolution, we developed a titration assay in which the two relevant ions are added simultaneously at a slow rate of typically 0.1 mL/min into a reservoir of water (i.e., co-titration of $CaCl_2$ and Na_2SO_4 stock solutions into H_2O) at a constant pH of 8.0 in the absence of atmospheric CO_2 (to avoid potential carbonation). In this way, the level of (super)saturation with respect to gypsum increases gradually at an equimolar Ca^{2+} : SO_4^{2-} ratio, and the different stages of crystallization can thus be followed on-line by immersing various sensors into the reactor, yielding time-dependent profiles as exemplified in Figure 1. The entire setup is depicted schematically in the Supporting Information (SI; Figure S1) and was conceived in analogy with titration methodologies reported in the literature for other minerals like calcium carbonate.[40] Measuring the concentration of free calcium ($c_{free}(Ca^{2+})$) as a function of time by means of an ion-selective electrode (ISE) leads to classical LaMer-type diagrams, as shown in Figure 1a: the amount of free Ca^{2+} ions increases until a deflection point is reached, which denotes the onset of ample precipitation that subsequently reduces the level of dissolved calcium (and sulfate) towards the solubility of the formed solid phase, which agrees reasonably well with values expected for gypsum at the given salinity and temperature (ca. 23 mM $CaSO_4$).[41] Hereinafter, solutions with free calcium concentrations below and above the latter value (as indicated by the dashed green line in Figure 1a) will be referred to as nominally under- and supersaturated, respectively.

Prior to the deflection point, the detected concentration of free calcium ions is significantly lower than expected based on the dosed amounts (grey line in Figure 1a), both below and above the nominal level of saturation (reached at $c_{added}(Ca^{2+}) \approx 0.032$ M). This indicates that Ca^{2+} and SO_4^{2-} ions exist in equilibrium with ion pairs ($CaSO_4^0$) and, potentially, also larger clusters (e.g., $[CaSO_4^0]_n$). The presumed 1:1 stoichiometry of these species can be directly verified by combining the Ca-ISE data with the simultaneously measured conductivity (κ) of the solution. The obtained binding profiles (Figure 1b) confirm that equimolar quantities of Ca^{2+} and SO_4^{2-} reside in the associated species in the pre-nucleation stage (as well as during and after

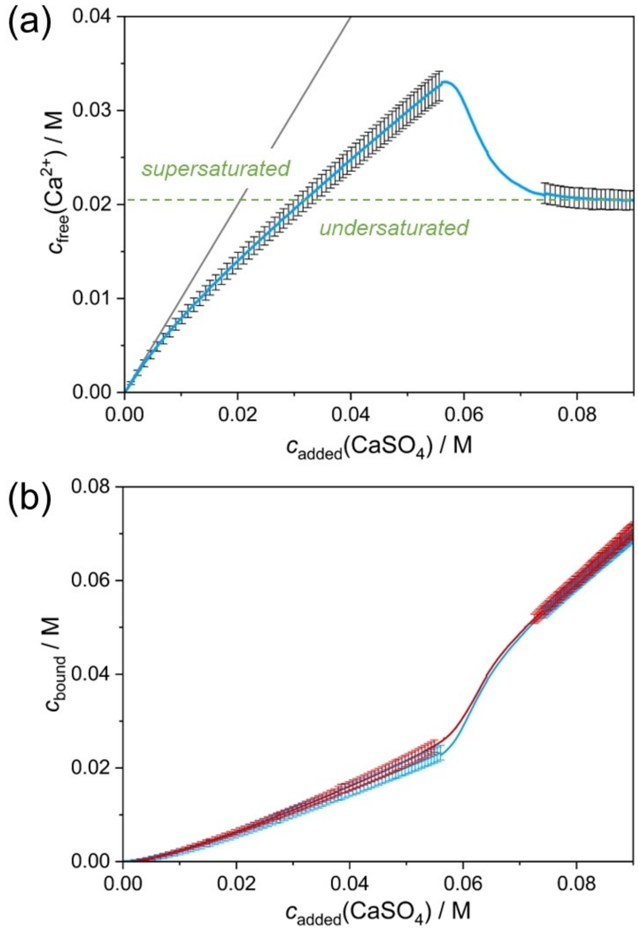

Figure 1. In situ monitoring of calcium sulfate crystallization from aqueous solution at ambient conditions by means of stoichiometric co-titration. (a) Concentration of free calcium ions measured by an ion-selective electrode (ISE) during simultaneous addition of 0.4 M $CaCl_2$ and 0.4 M Na_2SO_4 stock solutions into a reservoir of water (initial volume: 50 mL) at individual dosing rates of 0.1 mL/min and a constant pH of 8.0 (achieved by automatic counter-titration of 0.01 M NaOH). The blue line represents average values of $c_{free}(Ca^{2+})$ from five independent experiments with corresponding (± 1-σ) standard deviations, while the grey line indicates the actual amount of dosed calcium ions (i.e., $c_{added}(Ca^{2+})$). The separation of nominally under- and supersaturated solutions is marked by the dashed green line. (b) Binding patterns during co-titration obtained for calcium (blue) and sulfate (red) ions from ISE measurements (via $c_{bound}(Ca^{2+}) = c_{added}$-$(Ca^{2+})$ $c_{free}(Ca^{2+})$) and conductometry (see the Supporting Information for details), respectively. The shown curves represent average values from five independent experiments with corresponding (± 1-σ) standard deviations. Within experimental accuracy, equal amounts of Ca^{2+} and SO_4^{2-} ions are bound throughout all stages of the experiment. Note that error bars in (a) and (b) are omitted during the period of macroscopic precipitation (leading to a decrease in c_{free} and an increase in c_{bound}) due to the stochastic nature of the underlying nucleation processes and resulting large deviations between individual repetitions in this part of the curves.

nucleation), i.e., they are electroneutral on ergodic average ($c_{bound}(Ca^{2+}) \approx c_{bound}(SO_4^{2-})$) and do not contain significant amounts of HSO_4^-, in line with results of ab initio calculations and molecular dynamics (MD) simulations.[42] This is also intuitively expected in view of the strongly acidic character of sulfuric acid for both dissociation steps, which renders the speciation of the anion essentially independent of (relevant) pH levels. In fact, co-titrations performed at different pH between 3 and 10 gave identical results—within the limits of error and variations due to the stochastic nature of the occurring processes—as the experiments depicted by Figure 1 at pH 8 (see Figure S2 in the SI). The equilibrium constant of ion association determined from the present data ($K_A \approx 10^{2.2}$) agrees reasonably well with $CaSO_4$ ion pairing constants measured in earlier work ($K_A \approx 10^{2.15}$–$10^{2.30}$)[43-45] and shows that binding of Ca^{2+} and SO_4^{2-} is energetically less favorable than in the $CaCO_3$ case ($K_A \approx 10^3$–10^4),[8,46,47] likely due to a lower entropic contribution resulting from the hydration balance of free and bound ions.[47,48] More detailed analyses of the titration data according to the model of multiple binding equilibria[8] show that the average coordination number (N) of calcium and sulfate ions in bound states is ca. 1.2 and thus significantly higher than unity (see Figure S3 in the SI). This suggests that the under- and supersaturated solutions do not only contain mononuclear ion pairs (i.e., $CaSO_4^0$, for which $N = 1$), but must also include bi- or polynuclear clusters (e.g., chains of $[CaSO_4^0]$, for which $N(Ca^{2+}) = 2$)—much in line with the behavior reported for other minerals like $CaCO_3$[8,17] or $Ca(OH)_2$[49] in previous work.

To gain further insights into the degree of ion association and the size of the formed species, we performed analytical ultracentrifugation (AUC) on samples drawn at different times during the titration assay. The time-dependent sedimentation profiles detected by means of Rayleigh interference optics were fitted by a model assuming discrete and non-interacting species (see the Supporting Information for details). Best fit qualities were obtained for three distinct populations (P0, P1 and P2) in most cases. The resulting sedimentation coefficients (s), which discriminate the populations based on their (average) size, are displayed in Figure 2. Population P0 is detected at all sampled stages of the experiment and shows sedimentation coefficients in a rather narrow range of $s \approx 0.1$–0.2 S. This agrees well with values reported for spectator ions (i.e., Na^+ and Cl^-) in analogous AUC studies performed on the calcium carbonate system[8] and suggests that these ions do not participate in the association and dynamic exchange underlying the formation of larger clusters.[50] The latter processes involve free and bound Ca^{2+} and SO_4^{2-} ions, i.e. single ions, ion pairs and larger solute clusters, which constitute population P1, again in good agreement with observations made for $CaCO_3$.[8,50] Indeed, the fact that a single signal is obtained for this population could be interpreted as the existence of clusters with a defined size. However, this would contradict the current picture of PNC formation,[28] which has proven capable of predicting the experimentally determined limit for liquid-liquid phase separation in the case of calcium carbonate.[21] Therefore, the more likely explanation of the observed behavior is that the equilibria of ion association are very fast when compared to the timescale of the AUC experiment, which is on the order of hours.[50] Consequently, the measured signal represents the average size of all species

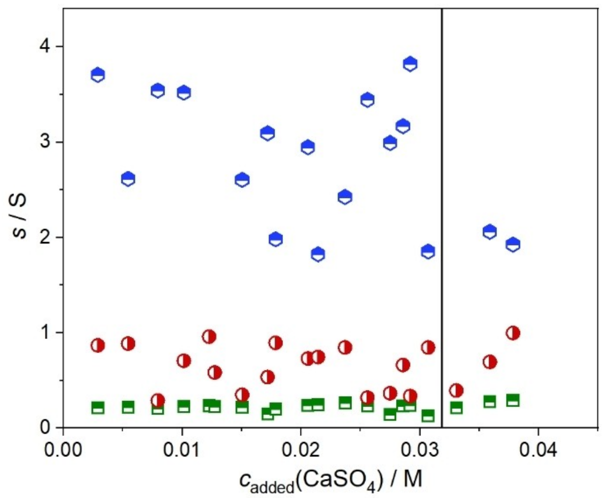

Figure 2. Detection of early precursors during $CaSO_4$ crystallization by analytical ultracentrifugation (AUC). Plot of the sedimentation coefficients determined at different stages of co-titration of 0.4 M $CaCl_2$ and 0.4 M Na_2SO_4 stock solutions into a reservoir of water (initial volume: 50 mL) at individual dosing rates of 0.02 mL/min and a constant pH of 8.0 (achieved by automatic counter-titration of 0.01 M NaOH). Three distinct populations were detected: spectator ions (P0, green squares), $CaSO_4$ ion pairs and solute clusters (P1, red circles), and phase-separated nanoparticles or -droplets (P2, blue diamonds). The vertical line indicates the transition from a nominally undersaturated system to a regime supersaturated with respect to the final crystalline phase (cf. Figure 1a). Note that no individual error bars are given because the errors resulting from the underlying fits are purely mathematical and do not provide reasonable estimates. Rather, the scatter of values from point to point for one population represent the range of the actual error (i.e., $\triangle s \approx 0.1$ S for P0, $\triangle s \approx 1$ S for P1, and $\triangle s \approx 1.5$ S for P2).

involved in the rapid equilibria, weighted according to the population of each state. The third detected population (P2) comprises significantly larger entities at $s \approx 2$–4 S, which apparently do not participate in the rapid equilibria of solute clustering described above and thus give a separate signal. This does not mean that the size distribution of these species is not controlled by similar (yet slower) chemical equilibria, although the structures might also be stabilized by kinetic factors (such as a transient charge limitation of growth). In any case, this larger population seems to disappear in the nominally supersaturated regime (likely due to growth or aggregation to sizes that are too large to be detected by AUC, as discussed further below). These latter species could be small $CaSO_4$ nanoparticles or strongly hydrated nanodroplets. Depending on their density (as given by the relative fractions of $CaSO_4$ units and hydration water),[51] they measure between 2 and 5 nm in size when assuming spherical shape; in the case of rods,[38,39] the measured sedimentation coefficients would translate into species with smaller dimensions due to the higher frictional ratio.[52]

In a second approach to characterize the species occurring during the early stages of calcium sulfate crystallization from solution, we performed in-situ small-angle X-ray scattering (SAXS) experiments using the co-titration setup described above coupled to a flow-through cell, which was aligned with a synchrotron-sourced X-ray beam. Representative results of these studies are summarized in Figure 3. Scattering patterns recorded at different times of the co-titration assay (Figure 3a) show a continuous evolution and confirm the presence of nanoscale crystallization precursors soon after the onset of the titration experiment (i.e., in solutions still undersaturated with respect to gypsum). This conclusion is evidenced by significant scattering from discrete species in the bulk ensemble, causing a change in the dependency of the scattering intensity $I(q)$ on the scattering vector q from $I(q) \propto q^{-1}$ for $q > 1\ nm^{-1}$ to $I(q) \propto q^0$ for $q < 1\ nm^{-1}$. Using a cylindrical form factor and assuming a polydisperse distribution (see the Supporting Information for details),[38] the best fit of the experimental scattering curves was obtained for a radius of $r = 0.1$ nm and a preferred length of $L \approx 1$ nm, as illustrated in Figure 3b. These species arguably correspond to population P2 traced by AUC (cf. Figure 2) as well as to the clusters of ca. 3 nm size observed by SAXS in our previous studies on supersaturated $CaSO_4$ solutions (with respect to gypsum) obtained by direct mixing instead of co-titration.[38,39] The time-dependent evolution of the volume fraction of P2 clusters can be inferred from the scattering intensity at $q = 0.9\ nm^{-1}$;[38] interestingly, corresponding plots (Figure 3c) show that the concentration of these species increases in the course of co-titration to reach a maximum, which occurs at about the same time as the drop in $c_{free}(Ca^{2+})$ (Figure 3c). This suggests strongly that the P2 clusters—i.e., pre-associated entities of $CaSO_4$—are actively involved in the process of crystal nucleation and possibly also the subsequent stages of growth. Finally, our in-situ SAXS experiments reveal the formation of another larger population (P3) at some point in the supersaturated regime before the maximum in $c_{free}(Ca^{2+})$, as evidenced by a significant increase in scattering intensity at $q < 1\ nm^{-1}$ that follows a dependency of $I(q) \propto q^{-a}$ (with $3 \leq a \leq 4$; cf. Figure 3a). We interpret this population as aggregates of P2 species, which (i) are too large to be detected by AUC (where simultaneously the P2 population disappears) and (ii) cause measurable optical turbidity in the system (as described below). In summary, the present analyses of solution speciation in the $CaSO_4/NaCl/H_2O$ system demonstrate that the ions undergo progressive association already in a regime of nominal undersaturation with respect to gypsum, yielding a dynamic population of ion pairs ($CaSO_4^0$) and neutral clusters ($[CaSO_4^0]_n$) in fast equilibrium with the free ions (P1) as well as a distinct fraction of larger species (P2), which grow and/or aggregate under supersaturated conditions into colloidal entities (P3).

Further key information about the crystallization process can be gained by tracing the evolution of optical turbidity of the solution during co-titration (Figure 4). Correlating the time-resolved transmittance signal (relative transmission τ) with the simultaneously measured calcium concentration and conductivity shows a clear and reproducible delay of about 750 s in the response to nucleation and growth of the solid phase: the solution becomes turbid long before the calcium concentration and the conductivity start to decrease. This implies that a significant volume fraction of particles large enough to scatter/absorb light (at $\lambda = 660$ nm) formed

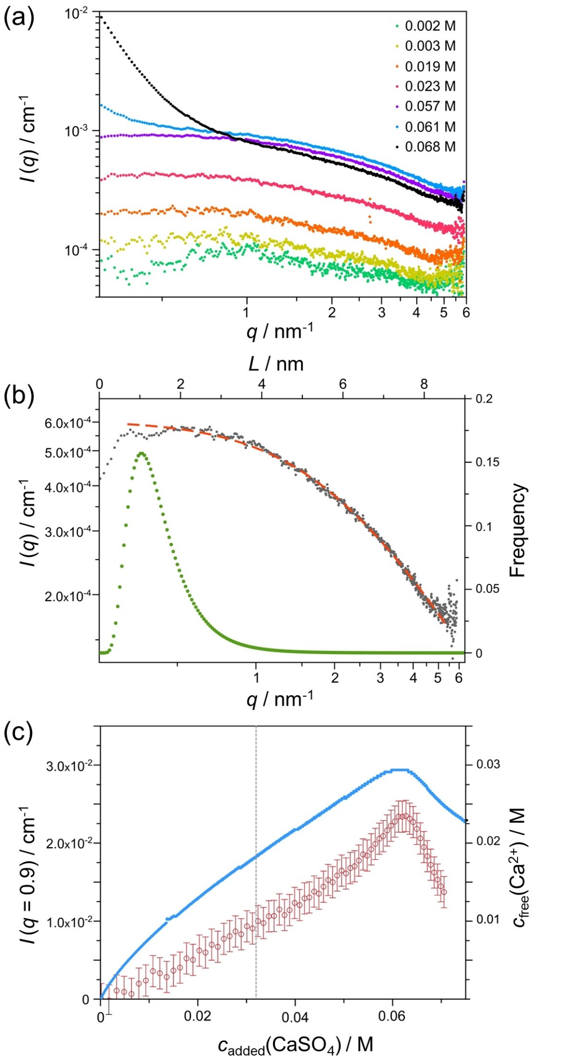

Figure 3. Time-resolved characterization of $CaSO_4$ clusters in under- and supersaturated aqueous solutions by in-situ small-angle X-ray scattering (SAXS) experiments. (a) SAXS patterns acquired at different times (as indicated by the corresponding values of $c_{added}(Ca^{2+})$) during a co-titration of 0.4 M $CaCl_2$ and 0.4 M Na_2SO_4 stock solutions into 50 mL water at individual dosing rates of 0.2 mL/min at pH 8. Scattering at high q originates from primary P2 clusters, while the increase of $I(q)$ at low q at later times suggest the presence of aggregates (P3). (b) Experimental SAXS pattern (black dots) obtained after 30 min (corresponding to $c_{added}(CaSO_4) = 0.039$ M), which was fitted (dashed red line) using a one-particle population that represents the P2 population dominating the scattering at high q. Assuming a diameter of 0.1 nm, the fit yields a log-normal size distribution (green dots) with a peak around 1 nm. (c) Evolution of the scattering intensity at $q = 0.9\ nm^{-1}$ as a function of added calcium and sulfate ions (red circles; average values with limits of uncertainty estimated via sensitivity analysis of the background subtraction procedure), as compared to the simultaneously measured progression of the free Ca^{2+} concentration (blue line; cf. Figure 1a). The vertical grey dotted line indicates the transition from a nominally undersaturated system to a regime supersaturated with respect to the final crystalline phase (cf. Figure 1a). It is important to note that the structural evolution as a function of time (and $c_{added}(Ca^{2+})$) cannot be directly compared to the results obtained by AUC (cf. Figure 2) and turbidimetric monitoring (cf. Figure 4) due to the different rates of reactant addition (with faster addition leading to higher $c_{added}(Ca^{2+})$ for species P2 and P3 to appear).

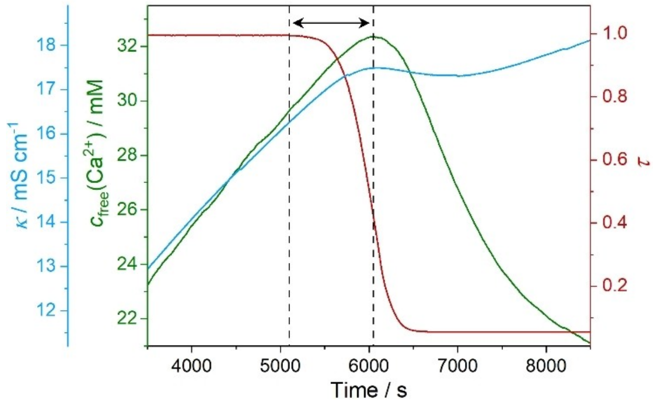

Figure 4. Experimental evidence for non-classical processes during nucleation of calcium sulfate from solution. Plot of the measured concentration of free calcium ions (green) together with the simultaneously monitored conductivity (blue) and optical transmission (red) as a function of time during co-titration of 0.4 M $CaCl_2$ and 0.4 M Na_2SO_4 stock solutions into 50 mL of water at individual dosing rates of 0.02 mL/min and a constant pH of 8.0. Note the significant time difference between the onset of detectable turbidity in the system and the (local) maxima in $c_{free}(Ca^{2+})$ and κ (indicated by dashed vertical lines and the arrow). The secondary increase in conductivity at $t > 7500$ s is due to the continuous addition of sodium and chloride counterions, which remain in solution during further growth of calcium sulfate particles.

without consuming any detectable amounts of the free ions in solution.

This observation has a number of important consequences:

(i) The maximum in the calcium potential does not signify the initial step of phase separation, as discussed for other mineral systems in previous studies;[40,49] rather, species constituting a separate phase have already formed at the time of measurable turbidity increase and likely even before, for example by liquid-liquid separation as shown for calcium carbonate.[21] In this sense, the maximum in the free concentration of calcium should be understood as the onset of the equilibration of the system towards the solubility product of gypsum.

(ii) The fact that visible precipitation does not lead to a sensible decrease in the concentration of free calcium (and sulfate) ions implies that the formed phase either cannot grow freely or constitutes a dense liquid that adjusts its composition according to the increasing ion activity product in the mother solution; in any case, the initially formed phase appears to be an intermediate that first needs to reorganize to yield crystalline gypsum (intrinsic growth inhibition; as discussed in further detail below).

(iii) The absence of any discontinuity (e.g., a kink) in the calcium potential at the onset of turbidity inevitably means that phase separation relies on *bound* species, i.e., pre-formed entities such as ion pairs and/or larger clusters, which are part of the bound population and thus not detected by the calcium ion-selective electrode.

(iv) Along the same lines, the lack of a kink in the conductivity profile proves that the species involved in phase separation are neutral on average, that is, the associated precursors do not need to include or release sulfate ions to form an—arguably neutral—separate phase.

We emphasize that all these conclusions directly follow from a correlation of the raw data and do not rely on any particular speciation model. Another immediate consequence of the experimental data is that the precursor species underlying the nucleation of gypsum are not (or rather no longer) in rapid equilibrium with the ions in solution, as otherwise their consumption upon phase separation would induce a shift in the equilibrium that should be detected by the ISE and the conductivity probe. This suggests that the species in question are the larger clusters (P2) detected by AUC and SAXS. Notably, the formation of these nanoscopic entities occurs in a continuous manner parallel or subsequent to equilibrium ion association in solution, as there is also no singularity in the calcium and conductivity profiles prior to nucleation. One possible explanation for this behavior is that the precursors result from nanoscopic liquid-liquid demixing (initiated much earlier than macroscopic precipitation) and have a partitioning coefficient very similar (or even identical) to the equilibrium constant of ion association in solution, as recently reported for calcium carbonate.[17,20,21,53] In this case, the population P2 would be droplets of the formed dense liquid phase—which intuitively is at odds with the anisotropy of P2 species suggested by the SAXS analyses. However, very recent work has shown that phases lacking any distinct crystalline order may well develop into anisotropic shapes.[54] In the present system, macroscopic phase separation (as indicated by the drop of solution transmittance) occurs once a critical concentration of the P2 species has been reached, presumably because the number density of dense liquid droplets becomes high enough to trigger coalescence. Alternatively, the anisotropic P2 species could represent solid calcium sulfate nanoparticles (possibly formed and then embedded within a preceding dense liquid phase), which assemble and transform into mature gypsum crystals via non-classical processes[27] above some critical concentration. In any case, the key role of the P2 species in the nucleation of solid calcium sulfate fundamentally challenges the meaning of supersaturation in its classical definition, which considers the concentration of free (rather than bound) ions to be the determining factor.[47]

The significant delay between the onset of turbidity and the decrease in the concentration of free ions was further investigated by means of cryo-transmission electron microscopy (cryo-TEM). For this purpose, samples were repeatedly drawn at different times during the lag period (i.e., the interval delimited by the vertical dashed lines in Figure 4) and vitrified to quench the reaction. In the following, we discuss the different structural stages resolved during the lag period in an extensive series of numerous cryo-TEM studies (Figure 5), noting that precise times of sampling are not meaningful as these stages typically occur in parallel throughout the probed solution volumes. However, each of the shown structures was observed multiple times in more than 20 independently replicated experiments and can thus be considered as representative snapshots of the processes at work in the studied system. In all vitrified samples, abundant nanoscopic species were detected with diameters ranging from 1 to 5 nm (Figure 5a), which agrees reasonably well with the population P2 observed by both AUC and SAXS. Although these species appear to be spherical in the cryo-TEM images, definite conclusions regarding their true shape are not possible due to limited contrast in edge regions against the electrolyte background (which also contains fairly high amounts of calcium and sulfate ions). In addition, these entities could be rather flexible and dynamic, as suggested by pair distribution function (PDF) analysis and MD simulations performed in a previous study on the $CaSO_4$/NaCl/H_2O system,[39] thus lacking a truly well-defined morphology and resembling the structural model of dynamically ordered liquid-like oxyanion polymers (DOLLOPs) proposed for calcium carbonate.[16] Moreover, there is likely a continuous transition in size between populations P1 (i.e., DOLLOPs) and P2 (primary $CaSO_4$ particles or droplets), which may therefore both contribute to the ensemble of nanodots resolved by cryo-TEM. In any case, the acquired images clearly show that these species tend to aggregate during the investigated period, forming irregular networks that extend over up to several hundreds of nanometers in solution (Figure 5b), which correspond to the larger population P3 detected by SAXS (cf. Figure 3a) and account for the observed macroscopic turbidity of the system (cf. Figure 4). The apparent density and overall shape of the aggregates vary from diffuse cloud-like structures over ill-defined granular textures to more compact spheroids (see Figure S4 in the Supporting Information for further images). All these structures do not produce any distinct diffraction spots, and hence can be considered as an amorphous phase lacking medium- to long-range order, which was also observed by X-ray scattering in our previous work[38,39] and other advanced techniques in a number of recent studies.[55–59] Interestingly, this intermediate disordered state appears to be somewhat different from other amorphous precursor phases (such as amorphous calcium carbonate (ACC) or amorphous calcium phosphate (ACP)), in a sense that the primary building units (i.e., P2 species) remain more or less individually separated inside their aggregates (cf. white circles in Figure 5b), i.e., they do not coalesce into one continuum, as already indicated by previous SAXS analyses.[38,39] This may be one reason why in the present work, unlike other studies,[58,59] this intermediate phase proved to be virtually impossible to isolate in the dry state by microfiltration (giving exclusively crystalline gypsum) or solvent quenching (yielding pure bassanite,[60,61] i.e., $CaSO_4\cdot 0.5H_2O$), suggesting a transient structure that only persists in a highly hydrated form.

The next step in the nucleation process is particularly intriguing: at some point, the primary species start to reassemble either within the disordered aggregates (Figure 5c)

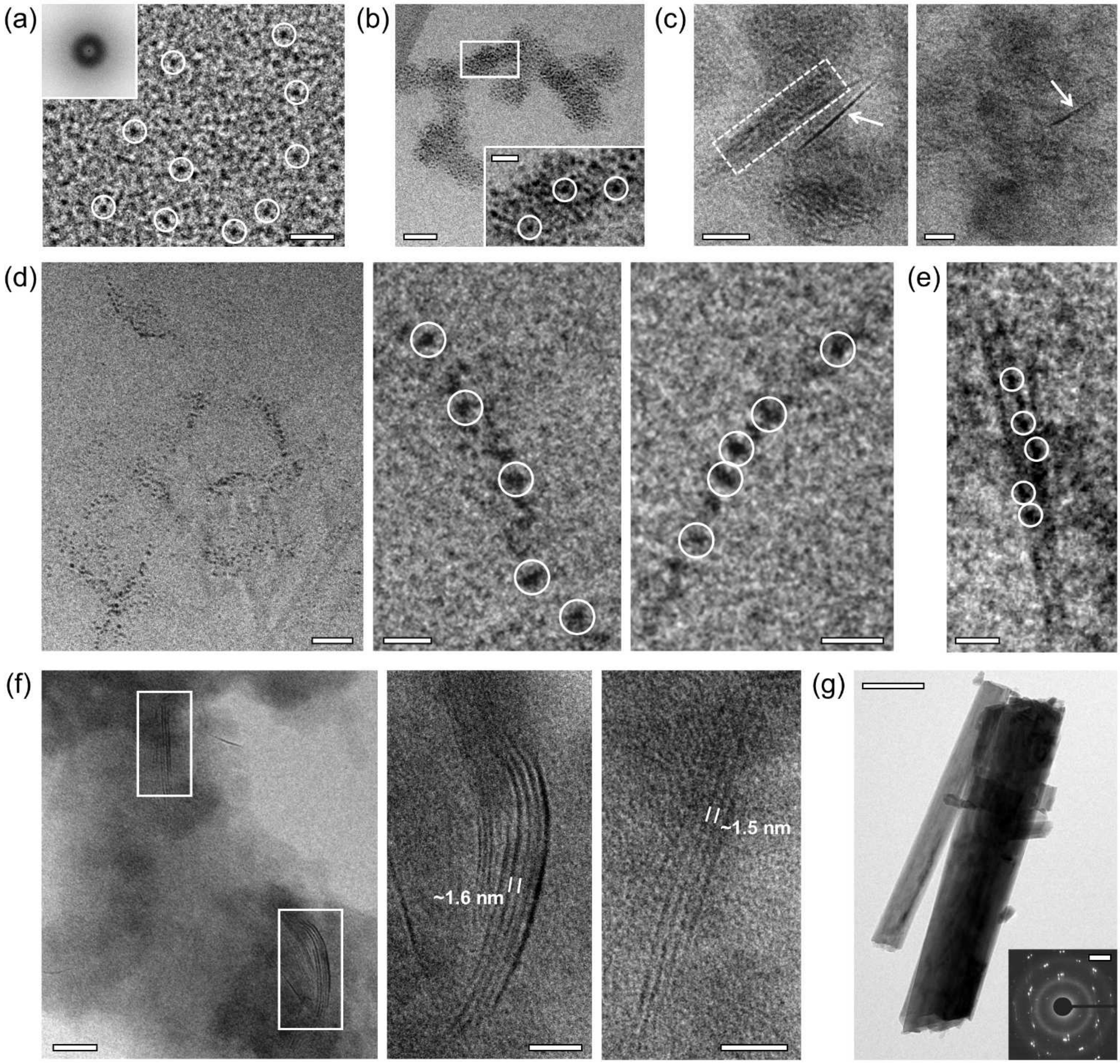

Figure 5. Direct visualization of the key stages in gypsum nucleation from solution by cryogenic transmission electron microscopy. All images were taken from vitrified aliquots drawn during the lag period of a co-titration experiment as indicated by the arrow in Figure 4, where the following stages were reproducibly observed in parallel throughout a given sample: (a) Nanosized primary species (exemplarily highlighted by white circles) with apparent diameters ranging from 1 to 5 nm as suggested by fast Fourier transformation (FFT) of the entire field of view (inset). The observed clusters likely correspond to populations P1 and, in particular, P2 as detected by AUC and SAXS. (b) Disordered aggregates of primary species (i.e., population P3), in which individual units can still be recognized as physically separated entities (highlighted by white circles in the inserted enlarged view of the area marked by the white rectangle). (c) Anisotropic structures (white arrows) formed within the disordered aggregates, along with an earlier stage of preferential orientation comprising a larger ensemble of primary species (dashed white rectangle). (d) Anisotropic structures formed in solution outside of the disordered aggregates (left panel), which are revealed to be one-dimensional chains of primary species at higher magnification (middle and right panels, where white circles highlight individually still separated units). (e) Co-oriented pair of nanocluster chains, marking the transition from 1D to 2D ordering. (f) Larger domains with periodic structuring formed within disordered "clouds" of primary species, likely as a result of progressive stacking of nanocluster chains into 2D arrays. The middle and right panels are close-up views of the areas delimited by white rectangles in the left panel, showing proto-lattices with spacings of ca. 1.5 and 1.6 nm, respectively. (g) Microscopic crystals displaying the typical habit of gypsum, which is confirmed as crystalline phase by electron diffraction (see Figure S7 in the Supporting Information for an assignment of the observed reflections). Scale bars are (a) 20 nm; (b) 20 nm (main image) and 5 nm (inset); (c) 20 nm; (d) 20 nm (left panel) and 5 nm (middle and right panels); (e) 5 nm; (f) 25 nm (left panel) and 10 nm (middle and right panels); (g) 200 nm (main image) and 2 nm^{-1} (inset).

or elsewhere in the solution (Figure 5d and Figure S5 in the SI), building anisotropic domains along one direction (i.e., individual nanodots aggregate in a one-dimensional fashion). Notably, the primary units do not merge upon ordering, i.e., they remain spatially separated and align much like pearls on a string. The observed elongated assemblies typically consist of 5–10 single units and extend over about 10–15 nm in length. These peculiar anisotropic interactions imply that the primary species must have some kind of internal structural order, which allows them to "feel" each other (e.g., through electrical dipoles) and thus adopt preferential orientations. A clue to these effects was provided in a recent study, which proposed the structure of the primary species to consist of square-shaped Ca-SO_4-Ca-SO_4 units, wherein six stacks are arranged in an AB pattern and each calcium ion is coordinated by two in-plane water molecules.[39] The role of the observed "nanocluster chains" in the process of calcium sulfate nucleation becomes evident from further cryo-TEM images collected during the lag period between the onset of turbidity and the decrease in $c_{\mathrm{free}}(Ca^{2+})$: once formed, the initial 1D structures begin to mutually interact and align laterally, first pairwise (Figure 5e) and later involving multiple individuals that stack into larger 2D arrays (Figure 5f and Figure S6 in the SI), usually nearby or embedded within the disordered precursors. Typical interlayer spacings measured in these assemblies range from 1.1 to 1.6 nm and thus are significantly larger than the longest regular distance in the structure of crystalline gypsum ($d=0.76$ nm for (020)), indicating the presence of excess hydration water in-between the $CaSO_4$-rich layers. Hence, the assembly of the initial 1D chains into 2D arrays seems to afford a proto-structure of the final crystalline phase. We consider this process—and/or the earlier emergence of 1D anisotropy—as a rate-limiting step in the formation of gypsum crystals, which explains the experimentally observed delay between the onset of turbidity and the decrease in the free calcium concentration and may be considered as the major barrier in gypsum crystallization. In other words, the re-organization of the initially disordered $CaSO_4$ precursors into ordered domains intrinsically inhibits the crystallization of gypsum.

This notion is further corroborated by the fact that the next stage captured in the cryo-TEM analyses already reveals micron-sized particles, which display well-defined diffraction patterns with reflections matching those of crystalline gypsum (Figure 5g and Figures S7–S10 in the SI). This means that once the barrier to the formation of a (proto-)lattice has been overcome and (more or less) crystalline surfaces are established, growth proceeds rapidly due to the high amount of potential growth units (free ions and their associated states in equilibrium) in close vicinity of the newly "born" nucleus. Analytically, this final stage of the nucleation process becomes manifest in a drop of the free calcium concentration towards the solubility of gypsum (cf. Figure 1), which is accompanied by a significant decrease of both solution conductivity (cf. Figure 4) and the volume fraction of population P2 in the SAXS experiments (cf. Figure 3c). The latter feature indicates that pre-formed primary species are incorporated into the emerging structure of gypsum,[38] while the drop in $c_{\mathrm{free}}(Ca^{2+})$ and κ suggests that free calcium and sulfate ions are consumed quickly as the nucleated crystals grow. Previous work has shown that, under the given conditions, growth of gypsum faces occurs mainly through 2D nucleation and subsequent step advancement.[62] This would imply that the cascade of processes underlying the non-classical crystallization of gypsum ends with a "classical" stage of growth through ion-by-ion addition—a notion that clearly requires further investigations.

Summary and Conclusions

In recent years, significant progress has been made in our understanding of the mechanistic, thermodynamic and kinetic principles governing the precipitation of calcium sulfate from solution[32,33] and a number of so-called "non-classical" precursors were reported, including nanometric primary particles,[38,39,56,58,59] amorphous or disordered phases,[38,39,52–56] mesocrystalline textures[60,61] interspersed with amorphous domains,[63,64] as well as crystalline intermediates.[55,61] In the present work, we have established a detailed view of the entire process of gypsum nucleation from aqueous solutions at ambient conditions. This became possible through the development of a potentiometric co-titration assay and its combination with in-situ turbidimetric and conductometric monitoring as well as high-resolution techniques such as AUC, SAXS and cryo-TEM. In particular, the cryo-TEM images acquired during the identified "lag period" allowed for a direct visualization of the crucial steps of solution-mediated calcium sulfate crystallization, namely the emergence of order in an initially disordered environment and the formation of the first (proto-)lattice, i.e. the actual crystalline nucleus.

A summary of the observed complex pathway is provided as a schematic drawing in Figure 6. In a solution undersaturated with respect to gypsum—created by slow and simultaneous addition of $CaCl_2$ and Na_2SO_4 into water—free calcium and sulfate ions form certain amounts of ion pairs[43–45] in a medium rich in spectator ions (Na^+ and Cl^-, P0 in AUC), but also populate higher degrees of association, i.e., solute bi- or polynuclear clusters that are charge-neutral on ergodic average, as shown by potentiometric and conductometric analysis. These species, which were previously predicted by simulation,[42] coexist in equilibrium in the one-phase system and constitute population P1 detected by AUC, with individual fractions determined by the respective association constants. Besides these solute entities, a discrete population of nanometric clusters is observed from the beginning of the co-titration experiment on (denoted as P2 in the AUC results). Since these larger clusters can already be detected in very dilute solutions far below the solubility of gypsum, they appear to exist as a less dynamic pseudo-phase in the homogeneous system, which cannot grow to macroscopic sizes and does not participate in the fast equilibria of the dissolved species. The P2 population is independently observed by in-situ SAXS analyses and may, or may not, be formed by structural

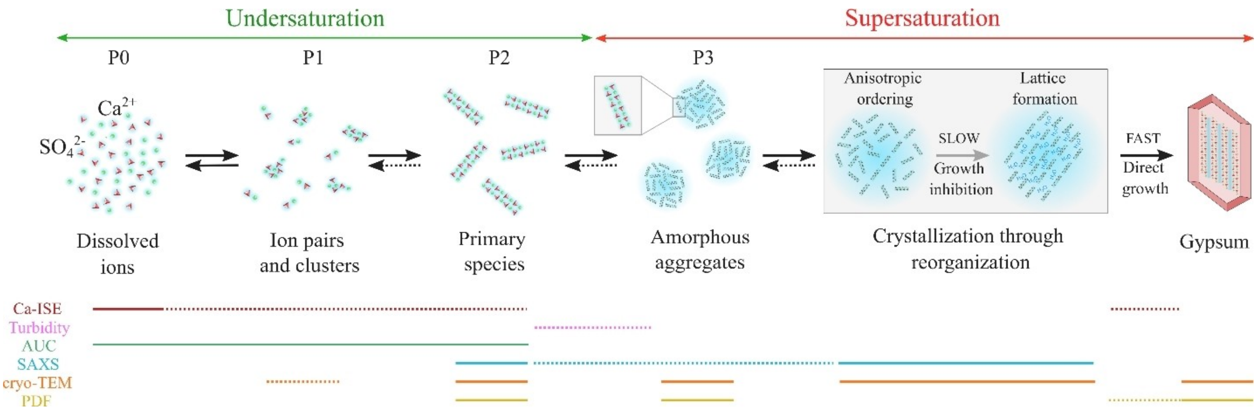

Figure 6. Holistic model of gypsum nucleation from aqueous solution at ambient conditions. (Top) Schematic drawings of the key stages observed in the present work on the way from dissolved ions to crystalline gypsum particles throughout the nominally under- and supersaturated regimes. For detailed explanations see text. (Bottom) Characterization methods used to capture and analyze the different stages, where full lines indicate direct and detailed insights into the respective processes while indirect evidence is represented by dashed lines. Note that pair-distribution function (PDF) analysis was included as another powerful technique for $CaSO_4$ precursor characterization, which was not applied in the present work but is documented in detail elsewhere.[39]

changes of polynuclear species in the P1 population (i.e., pre-nucleation clusters in a broader sense).[21] In any case, the SAXS (and AUC) data indicate that P2 species persist in solution and do not noticeably change their size in the supersaturated regime. While cryo-TEM images suggest that these species are more or less spherical, fitting of the SAXS data provides evidence for an anisotropic, rod-like shape and a molecular structure as described in detail elsewhere.[38,39]

At some critical volume density, the P2 species start to aggregate into various disordered domains, as resolved by SAXS (population P3) and visualized by cryo-TEM. Macroscopically, this aggregation step causes visual turbidity in the solution, which can be quantified by the immersed optical probe. In turn, the process does not lead to any discontinuities in the measured free calcium concentration and conductivity, but it reduces the amount of discrete P2 species below the detection limit of AUC. These latter observations demonstrate that aggregation involves pre-associated ions and yields a disordered phase, which cannot grow by addition of further ions. Both SAXS and cryo-TEM confirm that the primary units are still separate entities within their aggregates and remain so until a crystal lattice is formed and growth can proceed, as indicated by a drop in the free calcium concentration and a concurrent decrease of the scattering intensity from P2 species in the SAXS patterns. Thus, the actual process of crystallization occurs through re-structuring of nanosized primary units inside their aggregates and subsequent coalescence. In the present work, this internal re-organization could for the first time be captured by vitrification and cryogenic transmission electron microscopy, allowing the birth of a crystal to be directly watched. The acquired images intriguingly show that re-organization takes place in (at least) two steps: first, one-dimensional anisotropy emerges as (still) separated individual nanoclusters line up in a more or less linear fashion. Subsequently, these 1D chains undergo further assembly by lateral stacking into bi- and multilayers, which initially show mutual distances significantly larger than lattice spacings observed in crystalline gypsum. This suggests the formation of a proto-lattice, which displays clear internal order but probably still contains excess water that must be released before a truly crystalline phase can be established. Once this is achieved, the high local concentration of $CaSO_4$ species in the surrounding "amorphous" environment causes rapid growth into micron-sized particles with the characteristic morphology of gypsum, which produce well-defined spots in electron diffraction patterns. The latter finding is consistent with previous observations made by cryo-TEM[56] as well as in-situ data obtained by means of wide-angle X-ray scattering (WAXS),[65] pair distribution function (PDF) analysis,[39] and Fourier transform infrared (FTIR) spectroscopy[57] in earlier work. Thus, there is comprehensive evidence that under the given conditions, the formation of gypsum is preceded by amorphous precursors and does not involve other (crystalline) phases. Most importantly, the insights gained in the present work suggest that structural re-organization from disordered aggregates of P2 species into (pseudo-)crystalline lattices is rather slow and thus impedes gypsum crystallization by posing an intrinsic barrier, which results from the very nature of the particle-based nucleation process. This "auto-inhibition" is so pronounced that already during the lag period between the responses of the turbidimetric and potentiometric sensors, some large gypsum crystals can be observed floating in the otherwise isotropically turbid system (see Figure S11 in the SI). This means that, due to intrinsic crystallization inhibition, only few nuclei have overcome the barrier to re-organization at this point while many other local events are still ongoing elsewhere in solution. In other words, gypsum crystals truly have a hard time forming from their disordered precursors, mainly because "getting started"—i.e., generating a nucleus for crystalline ordering—appears to be so inherently difficult.

Although the mechanisms depicted in Figure 6 and the experimental evidence provided by the data in Figures 1–5 establish a thorough picture of the crystallization pathway of gypsum from aqueous solutions at ambient conditions, there is still a number of fundamental aspects that require further investigation to attain complete understanding. These include, but are not limited to, (i) the determination of relative (meta)stabilities for the primary species, and the driving force(s) triggering their initial aggregation and later re-organization; (ii) the importance of kinetic (e.g., desolvation of ions, ion pairs and clusters) and thermodynamic (e.g., interfacial free energies) barriers in controlling phase selection and crystallization rates of calcium sulfate minerals in natural and engineered environments; (iii) the potential role of the different types of nanoclusters during the growth of gypsum crystals; and (iv) the question as to whether the lessons learnt for the calcium sulfate system can be used to fill in the missing pieces in the nucleation pathways of other minerals such as calcium carbonate or phosphate. From a more applied perspective, the insights gained in this work could enable a more rational choice of crystallization modifiers for specific use cases such as the design of more sustainable construction materials,[66,67] or environmentally less critical solutions for scale inhibition.[68]

Supporting Information

The authors have cited additional references within the Supporting Information.[69–75]

Acknowledgements

The authors are deeply grateful to Prof. Helmut Cölfen (University of Konstanz) for his support and guidance throughout this work. We also thank Dr. Andreas Kempter and Dr. Volodymyr Boyko (both BASF SE) for their valuable contributions during the early stages of the project. SAXS experiments were performed at beamline ID02 of the European Synchrotron Radiation Facility (ESRF). Parts of this work were funded by BASF SE in the framework of a collaboration with the University of Konstanz. A.E.S.V.D. and A.F.M. acknowledge funding from the Consejería de Universidad, Investigación e Innovación, the competent authority in R&D of the Junta de Andalucía through project PROYEXCEL 00771 – SMART-water. Open Access funding enabled and organized by Projekt DEAL.

Conflict of Interest

The authors declare no conflict of interest.

Data Availability Statement

The data that support the findings of this study are available from the corresponding author upon reasonable request.

Keywords: Crystallization · Nucleation · Calcium sulfate · Gypsum · Supersaturation

[1] A. E. S. Van Driessche, M. Kellermeier, L. G. Benning, D. Gebauer, *New Perspectives on Mineral Nucleation and Growth*, Springer, Basel, **2017**.
[2] T. H. Zhang, X. Y. Liu, *J. Am. Chem. Soc.* **2007**, *129*, 13520.
[3] J. Russo, H. Tanaka, *MRS Bull.* **2016**, *41*, 369–374.
[4] Y. Jiang, M. Kellermeier, D. Gebauer, Z. Lu, R. Rosenberg, A. Moise, M. Przybylski, H. Cölfen, *Nat. Commun.* **2017**, *8*, 15933.
[5] Y. Tsarfati, S. Rosenne, H. Weissman, L. J. W. Shimon, D. Gur, B. A. Palmer, B. Rybtchinski, *ACS Cent. Sci.* **2018**, *4*, 1031.
[6] A. E. S. Van Driessche, P. H. H. Bomans, R. R. M. Joosten, D. Gil-Carton, N. A. J. M. Sommerdijk, M. Sleutel, *Nature* **2018**, *556*, 89.
[7] T. M. Tracy, T. O. Drews, H. Ramanan, C. He, J. Dong, H. Schnablegger, M. A. Katsoulakis, E. Kokkoli, A. V. McCormick, R. L. Penn, M. Tsapatsis, *Nat. Mater.* **2006**, *5*, 400.
[8] D. Gebauer, A. Völkel, H. Cölfen, *Science* **2008**, *322*, 1819.
[9] A. E. S. Van Driessche, L. G. Benning, J. D. Rodriguez-Blanco, M. Ossorio, P. Bots, J. M. Garcia-Ruiz, *Science* **2012**, *336*, 69.
[10] W. E. J. M. Habraken, J. Tao, L. J. Brylka, H. Friedrich, L. Bertinetti, A. S. Schenk, A. Verch, V. Dmitrovic, P. H. H. Bomans, P. M. Frederik, J. Laven, P. van der Schoot, B. Aichmayer, G. de With, J. J. De Yoreo, N. A. J. M. Sommerdijk, *Nat. Commun.* **2013**, *4*, 1507.
[11] J. Baumgartner, A. Dey, P. H. H. Bomans, C. Le Coadou, P. Fratzl, N. A. J. M. Sommerdijk, D. Faivre, *Nat. Mater.* **2013**, *12*, 310.
[12] B. Ludi, M. Niederberger, *Dalton Trans.* **2013**, *42*, 12554.
[13] M. H. Nielsen, S. Aloni, J. J. De Yoreo, *Science* **2014**, *345*, 1158.
[14] N. D. Loh, S. Sen, M. Bosman, S. F. Tan, J. Zhong, C. A. Nijhuis, P. Kral, P. Matsudaira, U. Mirsaidov, *Nat. Chem.* **2017**, *9*, 77.
[15] R. E. Schreiber, L. Houben, S. G. Wolf, G. Leitus, Z. L. Lang, J. J. Carbo, J. M. Poblet, R. Neumann, *Nat. Chem.* **2017**, *9*, 369.
[16] R. Demichelis, P. Raiteri, J. D. Gale, D. Quigley, D. Gebauer, *Nat. Commun.* **2011**, *2*, 590.
[17] D. Gebauer, M. Kellermeier, J. D. Gale, L. Bergström, H. Cölfen, *Chem. Soc. Rev.* **2014**, *43*, 2348.
[18] P. J. M. Smeets, A. R. Finney, W. E. J. M. Habraken, F. Nudelman, H. Friedrich, I. Laven, J. J. De Yoreo, P. M. Rodger, N. A. J. M. Sommerdijk, *Proc. Natl. Acad. Sci. USA* **2017**, *114*, E7882.
[19] M. A. Bewernitz, D. Gebauer, J. Long, H. Cölfen, L. B. Gower, *Faraday Discuss.* **2012**, *159*, 291.
[20] A. F. Wallace, L. O. Hedges, A. Fernandez-Martinez, P. Raiteri, J. D. Gale, G. Y. Waychunas, S. Whitelam, J. A. Banfield, J. J. De Yoreo, *Science* **2013**, *341*, 885.
[21] J. T. Avaro, S. L. P. Wolf, K. Hauser, D. Gebauer, *Angew. Chem. Int. Ed.* **2020**, *59*, 6155.
[22] J. H. E. Cartwright, A. G. Checa, J. D. Gale, D. Gebauer, C. I. Sainz-Diaz, *Angew. Chem. Int. Ed.* **2012**, *51*, 11960.
[23] H. Du, E. Amstad, *Angew. Chem. Int. Ed.* **2019**, *59*, 1798–1816.
[24] S. M. Clark, B. Colas, D. E. Jacob, J. C. Neuefeind, H. W. Wang, K. L. Page, A. K. Soper, P. I. Schodder, P. Duchstein, B. Apeleo-Zubiri, T. Yokosawa, V. Pipich, D. Zahn, E. Spiecker, S. E. Wolf, *Sci. Rep.* **2022**, *12*, 6870.
[25] T. A. Grünewald, S. Checchia, H. Dicko, G. Le Moullac, M. Sham Koua, J. Vidal-Dupiol, J. Duboisset, J. Nouet, O. Graubry, M. Di Michiel, V. Chamard, *Proc. Natl. Acad. Sci. USA* **2022**, *119*, e2212616119.

[26] J. J. De Yoreo, *Proc. Natl. Acad. Sci. USA* **2022**, *119*, e2121661119.
[27] J. J. De Yoreo, P. U. P. A. Gilbert, N. A. J. M. Sommerdijk, R. L. Penn, S. Whitelam, D. Joester, H. Z. Zhang, J. D. Rimer, A. Navrotsky, J. F. Banfield, A. F. Wallace, F. M. Michel, F. C. Meldrum, H. Cölfen, P. M. Dove, *Science* **2015**, *349*, aaa6760.
[28] D. Gebauer, P. Raiteri, J. D. Gale, H. Cölfen, *Am. J. Sci.* **2018**, *318*, 969.
[29] E. Macias-Sanchez, M. G. Willinger, C. M. Pina, A. G. Checa, *Sci. Rep.* **2017**, *7*, 12728.
[30] B. Jin, Z. Liu, C. Shao, J. Chen, L. Liu, R. Tang, J. J. De Yoreo, *Cryst. Growth Des.* **2021**, *21*, 5126.
[31] M. Sleutel, A. E. S. Van Driessche, *Nanoscale* **2018**, *10*, 12256–12267.
[32] A. E. S. Van Driessche, T. M. Stawski, M. Kellermeier, *Chem. Geol.* **2019**, *530*, 119274.
[33] A. E. S. Van Driessche, T. M. Stawski, L. G. Benning, M. Kellermeier, *Calcium Sulfate Precipitation throughout its Phase Diagram, in New Perspectives on Mineral Nucleation and Growth* (Eds.: A. E. S. Van Driessche, M. Kellermeier, L. G. Benning, D. Gebauer), Springer, Basel, **2017**.
[34] R. Sharpe, G. Cork, *Gypsum and anhydrite, in Industrial Minerals and Rocks* (Ed.: J. E. Kogel), 7th edition, Society for Mining, Metallurgy and Exploration Inc., Englewood, **2006**.
[35] K. S. S. Christie, T. Horseman, R. Wang, C. Su, T. Tong, S. Lin, *Desalination* **2022**, *525*, 115499.
[36] J. K. Warren, *Earth-Sci. Rev.* **2010**, *98*, 217.
[37] Q. Ma, H. He, Y. Liu, C. Liu, V. H. Grassian, *Phys. Chem. Chem. Phys.* **2013**, *15*, 19196.
[38] T. M. Stawski, A. E. S. Van Driessche, M. Ossorio, J. D. Rodriguez-Blanco, R. Besselink, L. G. Benning, *Nat. Commun.* **2016**, *7*, 11177.
[39] T. M. Stawski, A. E. S. Van Driessche, R. Besselink, E. H. Byrne, P. Raiteri, J. D. Gale, L. G. Benning, *J. Phys. Chem. C.* **2019**, *123*, 23151.
[40] P. I. Schodder, M. B. Gindele, A. Ott, M. Rückel, R. Ettl, V. Boyko, M. Kellermeier, *Phys. Chem. Chem. Phys.* **2022**, *24*, 9978.
[41] D. L. Parkhurst, *User's Guide to PHREEQC—A Computer Program for Speciation, Reaction-Path, Advective-Transport, and Inverse Geochemical Calculations*, United States Geological Survey, Lakewood, **1995**.
[42] H. J. Li, D. Yan, H. Q. Cai, H. B. Yi, X. B. Min, F. F. Xia, *Phys. Chem. Chem. Phys.* **2017**, *19*, 11390.
[43] R. Bell, J. George, *Trans. Faraday Soc.* **1953**, *49*, 619.
[44] R. Kalyanaraman, L. B. Yeatts, W. L. Marshall, *J. Chem. Thermodyn.* **1973**, *5*, 899.
[45] Z. Dai, A. Kan, F. Zhang, M. Tomson, *J. Chem. Eng. Data* **2015**, *60*, 766.
[46] J. Y. Gal, J. C. Bollinger, H. Tolosa, N. Gache, *Talanta* **1996**, *43*, 1497.
[47] M. Kellermeier, A. Picker, A. Kempter, H. Cölfen, D. Gebauer, *Adv. Mater.* **2014**, *26*, 752.
[48] M. Kellermeier, P. Raiteri, J. K. Berg, A. Kempter, J. D. Gale, D. Gebauer, *ChemPhysChem* **2016**, *17*, 3535.
[49] B. Madeja, D. Gebauer, M. R. Marsiske, A. Ott, M. Rückel, R. Rosenberg, A. Baken, T. M. Stawski, A. Fernandez-Martinez, A. E. S. Van Driessche, H. Cölfen, M. Kellermeier, *Cem. Concr. Res.* **2023**, *173*, 107258.
[50] M. Kellermeier, H. Cölfen, D. Gebauer, *Investigating the Early Stages of Mineral Precipitation by Potentiometric Titration and Analytical Ultracentrifugation, in Research Methods in Biomineralization Science* (Ed.: J. J. De Yoreo), Methods in Enzymology, Vol. 532, **2013**, pp. 45–69.
[51] E. H. Byrne, P. Raiteri, J. D. Gale, *J. Phys. Chem. C* **2017**, *121*, 25956.
[52] A. Spinnrock, D. Schupp, H. Cölfen, *Small* **2018**, *14*, 1870244.
[53] F. Sebastiani, S. L. P. Wolf, B. Born, T. Q. Luong, H. Cölfen, D. Gebauer, M. Havenith, *Angew. Chem. Int. Ed.* **2017**, *56*, 490.
[54] C. Feng, B. Q. Lu, Y. Fan, H. Ni, Y. Zhao, S. Tan, Z. Zhou, L. Liu, J. A. Hachtel, D. Kepaptsoglou, B. Wu, D. Gebauer, S. He, F. Chen, *J. Colloid Interface Sci.* **2024**, *657*, 960.
[55] Y. W. Wang, Y. Y. Kim, H. K. Christenson, F. C. Meldrum, *Chem. Commun.* **2012**, *48*, 504.
[56] A. Saha, J. Lee, S. M. Pancera, M. F. Bräu, A. Kempter, A. Tripathi, A. Bose, *Langmuir* **2012**, *27*, 11182.
[57] R. Stach, P. Krebs, F. Jones, B. Mizaikoff, *CrystEngComm* **2017**, *19*, 14.
[58] C. Jia, L. Wu, Q. Chen, P. Ke, J. J. De Yoreo, B. Guan, *CrystEngComm* **2020**, *22*, 6805.
[59] C. Jia, L. Wu, J. L. Fulton, X. Liang, J. J. De Yoreo, B. Guan, *J. Phys. Chem. C* **2021**, *125*, 3415.
[60] U. Tritschler, M. Kellermeier, C. Debus, A. Kempter, H. Cölfen, *CrystEngComm* **2015**, *17*, 3772.
[61] A. E. S. Van Driessche, L. G. Benning, J. D. Rodriguez-Blanco, M. Ossorio, P. Bots, J. M. Garcia-Ruiz, *Science* **2012**, *336*, 69.
[62] A. E. S. Van Driessche, J. M. Garcia-Ruiz, J. M. Delgado-Lopez, G. Sazaki, *Cryst. Growth Des.* **2010**, *10*, 3909.
[63] T. M. Stawski, H. M. Freeman, A. E. S. Van Driessche, J. Hövelmann, R. Besselink, R. Wirth, L. G. Benning, *Cryst. Growth Des.* **2019**, *19*, 3714.
[64] T. M. Stawski, G. J. Smales, E. Scoppola, D. Jha, L. F. G. Morales, A. Moya, R. Wirth, B. R. Pauw, F. Emmerling, A. E. S. Van Driessche, *Proc. Natl. Acad. Sci. USA* **2021**, *118*, e2111213118.
[65] M. Ossorio, T. M. Stawski, J. D. Rodriguez-Blanco, M. Sleutel, J. M. Garcia-Ruiz, L. G. Benning, A. E. S. Van Driessche, *Minerals* **2017**, *7*, 140.
[66] S. Reigl, A. E. S. Van Driessche, J. Mehringer, S. Koltzenburg, W. Kunz, M. Kellermeier, *CrystEngComm* **2022**, *24*, 1529.
[67] M. Maslyk, Z. Dallos, S. Seiffert, T. Hieke, K. Petrovic, U. Kolb, M. Mondeshki, W. Tremel, *Adv. Funct. Mater.* **2022**, *32*, 2111852.
[68] P. Ramirez-Garcia, M. Duran-Olivencia, M. Kellermeier, A. E. S. Van Driessche, *Desalination* **2022**, *544*, 116128.
[69] F. Malatesta, R. Zamboni, *J. Solution Chem.* **1997**, *26*, 791.
[70] R. M. Fuoss, L. Onsager, *J. Phys. Chem.* **1957**, *61*, 668.
[71] A. Apelblat, *J. Solution Chem.* **2016**, *45*, 1130.
[72] S. Katayama, *J. Solution Chem.* **1976**, *5*, 241.
[73] P. Schuck, *Biophys. J.* **2000**, *78*, 1606.
[74] J. Ilavsky, P. R. Jemian, *J. Appl. Crystallogr.* **2009**, *42*, 347.
[75] P. Comodi, S. Nazzareni, P. F. Zanazzi, S. Speziale, *Am. Mineral.* **2008**, *93*, 1530.

Manuscript received: May 3, 2024
Accepted manuscript online: October 7, 2024
Version of record online: November 16, 2024